Green Chemistry

PAPER

View Article Online
View Journal | View Issue

Cite this: *Green Chem.*, 2024, **26**, 9330

Efficient hydrodeoxygenation of lignin-derived phenolic compounds under acid-free conditions over carbon-supported NiMo catalysts†

Shan Jiang,[a] Riyang Shu, *[b] Anqi Wang,[a] Zhuoli Deng,[a] Yuhong Xiao,[a] Jiajin Li,[a] Qingwei Meng[a,c] and Qian Zhang *[a,c]

High-quality liquid biofuels can be produced from renewable lignin-derived phenolic compounds through an efficient hydrodeoxygenation (HDO) process in which the traditional catalysts usually include metal sites and acid sites that catalyze the hydrogenation and deoxygenation procedures respectively. This work presents a novel acid-free Ni_xMo_yN/C catalyst from the perspective of green chemistry providing a new pathway for HDO of lignin-derived phenolic compounds that involves hydrogenation deoxygenation and hydrogenolysis at the same time. A series of Ni_xMo_yN/C catalysts were prepared by varying the Ni : Mo molar ratio among which the Ni_1Mo_3N/C catalyst showed the best HDO performance. Guaiacol could be completely converted at 260 °C after 4 h with 95.8% cyclohexane selectivity. In addition a small amount of benzene could be obtained as a valuable fuel additive by-product by altering the conventional HDO reaction path. By shortening the reaction time benzene could be obtained as an intermediate product with a relative high selectivity. Based on the characterizations using XRD BET SEM TEM XPS H_2-TPD and EPR, the results demonstrate that the multiple active components of the Ni_1Mo_3N/C catalyst allow it to efficiently catalyze the hydrogen activation and C–O bond cleavage even under acid-free conditions. The existence of the active phases of Ni Ni_2Mo_3N and β-Mo_2C as well as the interaction between Ni and Mo metals together contributed toward efficient HDO performance. Not only for the various phenolic model compounds the feasibility of Ni_1Mo_3N/C catalysts for upgrading raw lignin oil was also demonstrated with the hydrocarbon content increasing from 5.7% to 88.4%. Notably arenes accounted for 18.2% of the hydrocarbon products which confirmed the occurrence of hydrogenolysis in the catalytic process. This work provides a novel route for the conversion of lignin-derived phenolic compounds to produce high-quality hydrocarbon liquid biofuels especially the direct production of arene components.

Received 9th May 2024,
Accepted 16th July 2024

DOI: 10.1039/d4gc02298j

rsc.li/greenchem

Introduction

Carbon neutrality has become a common demand of the global community recently. In order to minimize carbon dioxide emissions the development and improvement of sustainable energy sources to replace petrochemical fuels have received considerable attention.[1] Biomass resources are widely researched and utilized because of their wide range of sources low prices and environmental friendliness.[2] As one of the three main components of biomass lignin has a high carbon and hydrogen content as well as a high calorific value which make it a promising raw material to produce high-quality liquid biofuels.[3] In order to facilitate the production of liquid biofuels solid lignin feedstock is usually transformed into a liquid product (usually called lignin oil) at first by using pyrolysis oxidation and reduction methods which consists of a large number of phenolic compounds.[4] However the direct usage of lignin oil for fuel is challenging due to its high oxygen concentration and low chemical stability. Therefore further refining of phenolic compounds derived from lignin is required.[5]

Hydrodeoxygenation (HDO) is a commonly used pathway to improve the quality of lignin-derived phenolic compounds and it mainly involves hydrogenation and deoxygenation procedures.[6] Catalysts are conducive to completing HDO reactions by lowering the reaction activation energy significantly. Metal sites catalyze the hydrogenation procedures while acid sites catalyze the deoxygenation procedure.[7] Heterogeneous catalysts are commonly employed in this process due to their good

[a]*School of Chemical Engineering and Light Industry, Guangdong University of Technology, Guangzhou 510006, China. E-mail: zhangqian@gdut.edu.cn*
[b]*Guangdong Provincial Key Laboratory of Functional Soft Condensed Matter, School of Materials and Energy, Guangdong University of Technology, Guangzhou 510006, PR China. E-mail: shuriyang@gdut.edu.cn*
[c]*Guangdong Provincial Laboratory of Chemistry and Fine Chemical Engineering Jieyang Center, Jieyang 515200, China*

†Electronic supplementary information (ESI) available. See DOI: https://doi.org/10.1039/d4gc02298j

recovery characteristic which is quite compatible with green chemistry principles.[8] The metal components of the catalyst are the key catalysis sites to accomplish the hydrogenation process. Many different types of metal-based catalysts have been studied including noble metals (like Pt Pd and Ru)[9,10] transition metals (like Ni Cu and Co)[11] and metal carbides (like Mo carbide).[12] Among these the high cost of noble metals prevents their widespread usage although they can show outstanding HDO catalytic performance under moderate reaction conditions. Transition metals possess low cost and capable catalytic activity compared to noble metals which has seen them attract much attention especially based on green chemistry and sustainability considerations.[11] In addition most of the reported studies have presented the formation of saturated hydrocarbons because metal-based catalysts usually have a good hydrogenation ability.[9,10] However with a view to practical application the usage of unsaturated aromatic additives in liquid fuels especially arenes can enhance the octane number of automotive fuels reduce the volatility and play a positive role in engine efficiency and its life span.

Transition metal catalysts with a single metal component generally lead to an inadequate HDO activity and efficiency.[13] To improve the original sites electronically and geometrically a second active component can be added. This strategy enables changing the surface state of the catalysts and can increase the catalytic activity product selectivity and stability.[14–16] Given the strong synergistic catalytic effects a number of bimetallic component catalysts have been studied for the HDO reaction.[17,18] For instance Wang *et al.* studied the catalytic performance of the bimetallic NiS_2/MoS_2 catalyst in the HDO conversion of guaiacol. Their results showed that the bimetallic component catalyst was more efficient than that of a single component under the same circumstances.[19] Also our previous study explored bimetallic Ru-based catalysts in the HDO of lignin-derived phenolic compounds and showed that the addition of Ni and Co metal to $Ru/SiO_2–ZrO_2$ catalysts can significantly improve their HDO activities promoted by the synergetic effect of the bimetal species.[20,21] Cheng *et al.* synthesized a series of $Fe–Co/SiO_2$ catalysts *via* an impregnation process. The bi-component metal-based catalyst system achieved a significantly higher hydrocarbon yield (22.4%) compared to the single-component catalyst.[22] Therefore the bimetal catalytic strategy provides an effective method to enhance the HDO performance.

The usage of metal–acid bifunctional catalysts can significantly enhance the deoxygenation of phenolic compounds.[23] However catalyst deactivation can also occur due to the fact that excessive acid sites induce a higher rate of coke formation.[24] Laurent *et al.* investigated the catalytic effect of $CoMo/Al_2O_3$ on the HDO of guaiacol. Due to the strong acidity of Al_2O_3 the substrate could easily adsorb on the support and condense to form char. They also found a low carbon number balance which indicated the formation of deposited carbon in the reaction.[25] Echeandia *et al.* discovered that less coke was formed during phenol HDO over an activated-carbon-loaded Ni–W catalyst than an alumina-loaded one.[26] To mitigate the negative effects of these polymerization products in the reaction system the use of an acid-free catalyst may be a solution. Also the preparation process of acid-free catalysts avoids potential harm to the environment and has benefits from both economic and green catalysis considerations due to eliminating the acid usage.

In this paper a series of NiMo-based bimetallic catalysts on a carbon support were synthesized without the addition of an acid component in line with a green chemistry perspective. The active species composition oxygen vacancy properties and NiMo intermetallic interactions could be modulated by varying the Ni : Mo ratio. The catalysts were then employed for the HDO reaction of lignin-derived phenolic compounds. A series of catalyst characterizations were carried out and the HDO performance of the different catalysts was compared in order to reveal the relationship between the catalysts' physicochemical properties and the reaction performance. Finally a potential catalytic reaction mechanism was proposed based on the characterization and experiment results.

Materials and methods

Materials

Guaiacol $NiCl_2·6H_2O$ $MoCl_5$ and $(NH_4)_6Mo_7O_{24}·4H_2O$ were obtained from Macklin Reagent. Glucose octane and other model compounds were provided by Aladdin Reagent Co. Ltd (Shanghai China). All the reagents were analytical grade and require no further purification. The raw lignin oil was prepared by the pyrolysis of rice husks in a tube furnace. Fractional condensation was used to extract the phenolic components.[27]

Catalyst preparation

A series of Ni_xMo_yN/C bimetallic nanocatalysts with different Ni/Mo molar ratios (x/y = 1 : 1 1 : 2 1 : 3 and 1 : 4) were prepared by a sol–gel method. First $NiCl_2·6H_2O$ (2.0 g) a certain amount of $(NH_4)_6Mo_7O_{24}·4H_2O$ and glucose (5.0 g) were sequentially dissolved in deionized water (30 mL) with continuous stirring to obtain a homogeneous solution. Subsequently the solution was heated to 90 °C and a mixed homogeneous gel was obtained. The gel was dried by removing the water at 80 °C. The dried solid was placed in a furnace and calcined at 500 °C for 2 h in a H_2 flow to obtain the catalyst. Compared to the Ni_1Mo_3N/C catalyst the Ni_1/C catalyst did not involve the incorporation of $(NH_4)_6Mo_7O_{24}·4H_2O$ and only Ni was retained among the key elements (Ni Mo and N). Similarly the Mo_3/C catalyst did not involve the incorporation of $NiCl_2·6H_2O$ and only Mo was retained as the key element. As for the preparation process of the Ni_1Mo_3/C catalyst the usage of $(NH_4)_6Mo_7O_{24}·4H_2O$ was replaced by $MoCl_5$ in order to remove N from the key elements and only keep the Ni and Mo elements.

Catalyst characterization

Using a monochromatic Cu Kα radiation source (λ = 0.15418 nm) a Mini-Flex 600 diffractometer was used to gather the powder X-ray diffraction (XRD) data. Brunauer–Emmett–

Teller (BET) surface area and pore-size distribution measurements were performed on Autosorb-iQ equipment based on the adsorption desorption of nitrogen at −196 °C. The morphology and microstructure of the samples were characterized by SEM (SU8010 Hitachi) at 5.0 kV. High-resolution transmission electron microscopy (HR-TEM) analysis was performed using a FEI Talos F200S instrument at 200 kV to examine the micromorphology of the catalysts. A Tecnai F20 device (produced by FEI Thermo) was used for the energy dispersive spectroscopy (EDS) analysis. X-Ray photoemission spectrometer (XPS) analysis was conducted on a Thermo Fisher Scientific K-Alpha instrument and all the binding energies were calibrated by the C 1s peak at 284.8 eV. The temperature-programmed desorption of H_2 (H_2-TPD) was carried out in a U-shaped quartz reactor on a ChemStar instrument to study the hydrogen-activation and -adsorption properties of the catalyst. The presence of oxygen vacancies was further indicated by electron spin resonance spectroscopy (EPR) analysis performed on a Bruker EMX PLUS instrument with a center field strength of 3502.00 G and a sweep width of 100.0 G.

HDO of lignin-derived phenolic compounds and raw lignin oil

A typical HDO reaction took place in a 70 ml 316L stainless steel autoclave reactor with magnetic stirring and using electric heater units manufactured by Anhui Chem-n Instrument Co. Ltd (Hefei). In a typical run 20 mL of *n*-octane solution and 0.1 g of guaiacol (or other phenolic compounds) as the reaction substrate were added to the autoclave as feedstock. At the same time 0.05 g of fresh catalyst was also put into the reactor. Then the reactor was flushed 5 times with high pressure H_2 and then sealed and brought up to a certain temperature (220–260 °C) at 5 °C min^{-1}. The reaction solution was then kept warm for a period under constant stirring at 1000 rpm. After cooling the reaction solution was filtered using a 0.22 μm filter tip and injected into a chromatography vial and analyzed to determine its liquid product composition. The liquid products were measured qualitatively using gas chromatography-mass spectrometry (GC-MS Thermo Fisher Science $Trace_1300$) and a TG-5Sil column as the chromatographic column. The oven temperature was set at 60 °C for 2 min then ramped up to 260 °C at a rate of 10 °C per min for another 10 min. The injector was run in split mode (5 : 1) using helium as the support gas at 280 °C. Quantitative measurements of the different components were performed using the same instrument and a modified FID detector and mass analyzer. The phenolic compound conversion and product selectivity were determined using eqn (1) and (2).

$$\text{Conversion}\,(\%) = \frac{\text{moles}_{\text{in}} - \text{moles}_{\text{out}}}{\text{moles}_{\text{in}}} \times 100\% \quad (1)$$

$$\text{Selectivity}\,(\%) = \frac{\text{moles}\,(\text{product})_i}{\sum \text{moles}\,(\text{product})} \times 100\% \quad (2)$$

As for the HDO reaction of raw lignin oil the substrate included a certain amount of phenolic compounds (about 0.15 g) which was extracted from 3 g raw lignin oil with 20 mL octane. Then the substrate and 0.05 g catalyst were added into the reactor and the reaction process was the same as that for the above HDO process of phenolic compounds. Considering the complexity of the lignin oil only semiquantitative measurements were conducted by GC-MS before and after the HDO reaction. The product content was calculated based on the proportions of the peak areas.

Results and discussion

Catalysts characterization

The XRD spectra of the Ni_xMo_yN/C catalysts with different Ni/Mo molar ratios were first investigated. As shown in Fig. 1(a) the Ni_1Mo_1N/C catalyst displayed typical characteristic peaks of metallic Ni as observed by the 2θ diffraction peaks of the standardized data of PDF(04-0850). Signals for the diffraction peaks belonging to Ni_2Mo_3N crystals were observed in the patterns for the Ni_1Mo_2N/C Ni_1Mo_3N/C and Ni_1Mo_4N/C catalysts according to the standardized data in PDF(89-4564). Among them the signals of the 2θ diffraction peaks at 40.8° 43.1° 45.3° 59.0° 72.6° and 77.4° were attributed to the (221) (310) (311) (331) (510) and (520) crystal planes respectively. The Ni metal peak in the Ni_1Mo_2N/C catalyst not only showed a reduced peak intensity but was also slightly shifted to the lower 2θ degree. This shift could be attributed to the reduction of the Ni nanoparticle size and lattice extension caused by the incorporation of Mo into the face-centered cubic (fcc) structure of the Ni metal phase.[28] In addition with the further increase in the Mo composition characteristic diffraction peaks attributed to β-Mo_2C as assigned by PDF (35-0787) were also found in the patterns of the Ni_1Mo_3N/C and Ni_1Mo_4N/C catalysts. Especially in the case of Ni_1Mo_3N/C catalyst the diffraction peaks of β-Mo_2C and Ni_2Mo_3N exhibited the most pronounced intensities and the most ordered lattice structures which would be conducive to improving the catalyst stability during the reaction process. The absence of metallic Ni was probably due to the tiny size of the Ni metal particles. The existence of the Ni_2Mo_3N phase also had a negative effect on the formation of the Ni metal crystal structure. In addition the XRD patterns of the Ni_1/C Mo_3/C and Ni_1Mo_3/C catalysts are presented in Fig. 1b and were used to explore their differences with that of the Ni_1Mo_3N/C catalyst. It can be seen that Ni_1/C contained only the Ni metal phase and Mo_3/C contained only the carbide species of Mo metal. Based on the comparisons of the Mo_3/C and Ni_1Mo_3/C catalysts the addition of Ni promoted the carburization process of the Mo metal.[29] Without the introduction of the N element the Ni_1Mo_3/C catalyst only showed weak diffraction peaks attributed to the Ni and MoC phase. The comparison of the Ni_1/C and Ni_1Mo_3/C catalysts demonstrated that the introduction of Mo metal could improve the dispersion of Ni metal particles. Overall by the interaction of Ni Mo N and C elements the Ni_1Mo_3N/C catalyst possessed an abundant active phase of Ni_2Mo_3N and β-Mo_2C as well as a high dispersion of Ni metal particles.

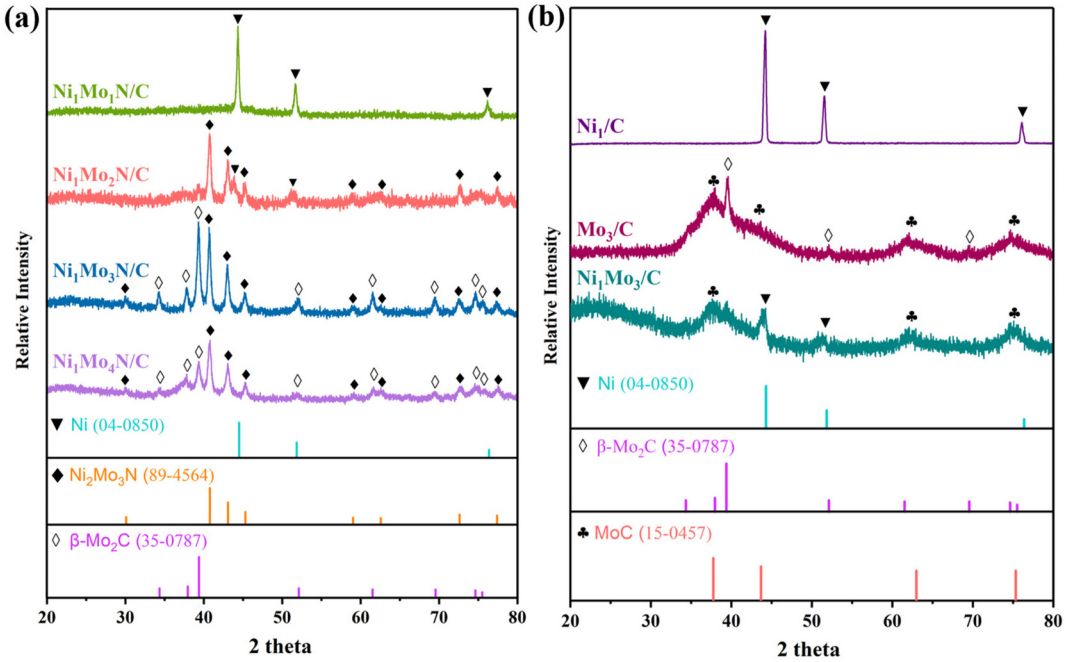

Fig. 1 (a) XRD patterns of the different Ni_xMo_yN/C catalysts. (b) XRD patterns of the Ni_1/C Mo_3/C and Ni_1Mo_3/C catalysts.

The specific surface area and pore structure of a catalyst have a significant impact on the exposure of active sites. The results from the N_2 porosimetry tests of the different Ni_xMo_yN/C catalysts are shown in Table 1 and Fig. S1.† Generally all the catalysts showed typical type IV isotherms and hysteretic rings in a high range of P/P_0 (Fig. S1†). Combined with the pore volume data in Table 1 mixed structures with mesopores and micropores were demonstrated. Among these catalysts the Ni_1Mo_3N/C catalyst had the largest mesopore volume value due to the enhanced formation of β-Mo_2C during calcination in which the Mo_2C phase is reported to have an abundant mesopore structure.[30,31] This result was also supported by the XRD analysis (Fig. 1). Moreover with the addition of excess Mo metals in the Ni_1Mo_4N/C catalyst both the specific surface area and the pore volume decreased including the mesopore volume. Overall the Ni_1Mo_3N/C catalysts had the largest mesopore volume value which is favorable for the adsorption and diffusion of large molecular substrates. The element content of the different prepared Ni_xMo_yN/C catalysts was also investigated. Based on the measurements by ICP-OES analysis and organic elemental analysis the results for the catalyst composition are listed in Table 1. It could be seen that the actual element content values were close to the theoretical ones and the Ni_1Mo_3N/C catalysts presented a Ni/Mo molecular ratio of 0.43.

The measurements for the catalyst morphology were conducted by SEM and TEM characterizations. The SEM images of the different catalysts are presented in Fig. 2 and Fig. S2† in which a large amount of granular material could be observed on the catalyst surface. Based on the XRD analysis these particles were probably metal Ni and Ni_2Mo_3N species. There was a tendency for the size of these particles to decrease with the increasing addition of the Mo metal element which may be related to the occurrence of a transition from Ni to Ni_2Mo_3N.

Table 1 Texture properties of the different Ni_xMo_yN/C catalysts

Catalysts	Surface area[a] ($m^2\ g^{-1}$)	Pore diameter[b] (nm)	Pore volume[c] ($cm^3\ g^{-1}$)			Element content (wt%)					
			V_{tot}	V_{mic}	V_{meso}	Ni[d]	Mo[d]	C[e]	N[e]	O[f]	Ni/Mo[g]
Ni_1Mo_1N/C	113	1.9	0.053	0.040	0.013	11.9	15.9	38.0	2.1	32.1	1.2
Ni_1Mo_2N/C	138	2.4	0.083	0.045	0.038	15.0	39.5	20.8	2.9	21.8	0.62
Ni_1Mo_3N/C	88	3.2	0.072	0.020	0.052	15.2	57.7	13.8	1.5	11.8	0.43
Ni_1Mo_4N/C	60	3.6	0.054	0.011	0.043	12.3	61.4	9.2	2.4	14.7	0.33

[a] MultiPoint Brunauer–Emmett–Teller (BET) method. [b] Barrett–Joyner–Halenda (BJH) method. [c] V_{tot}: total pore volume determined using density functional theory (DFT) and Boehm's titration. V_{mic}: micropore volume calculated using the *t*-plot method. V_{meso}: mesopore volume determined by the difference between V_{tot} and V_{mic}. [d] Ni and Mo contents in the catalysts determined by ICP-OES analysis. [e] C and N contents in the catalysts determined by organic elemental analysis. [f] Elemental oxygen content based on the difference between the other elements and the total. [g] Ni/Mo atomic ratios calculated from the ICP-OES results.

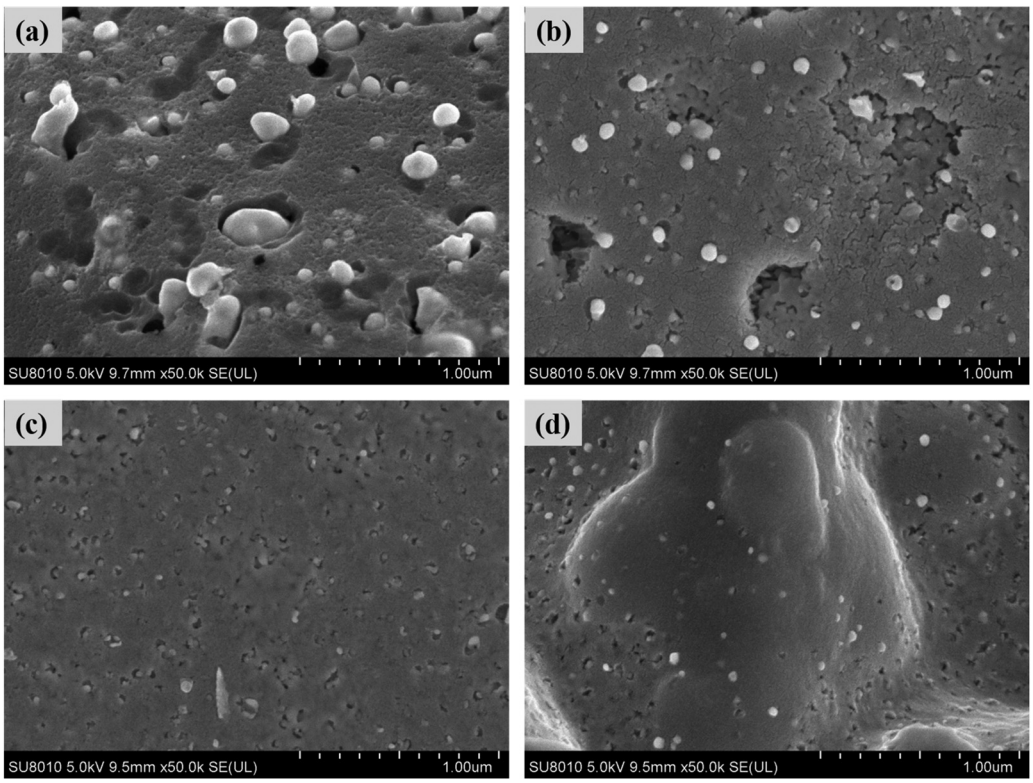

Fig. 2 SEM images of (a) Ni_1Mo_1N/C (b) Ni_1Mo_2N/C (c) Ni_1Mo_3N/C and (d) Ni_1Mo_4N/C catalysts.

Comparatively the Ni_1Mo_3N/C catalyst showed the smoothest surface and the smallest metal particle size. SEM-based EDS elemental analysis of the different Ni_xMo_yN/C catalysts was also carried out (Fig. S3–S6†). Each type of element was uniformly distributed on the catalyst surface indicating the effectiveness of the preparation method. To further understand the internal structure of these catalysts TEM characterization analysis was also performed (Fig. 3a–d). The dark region in these

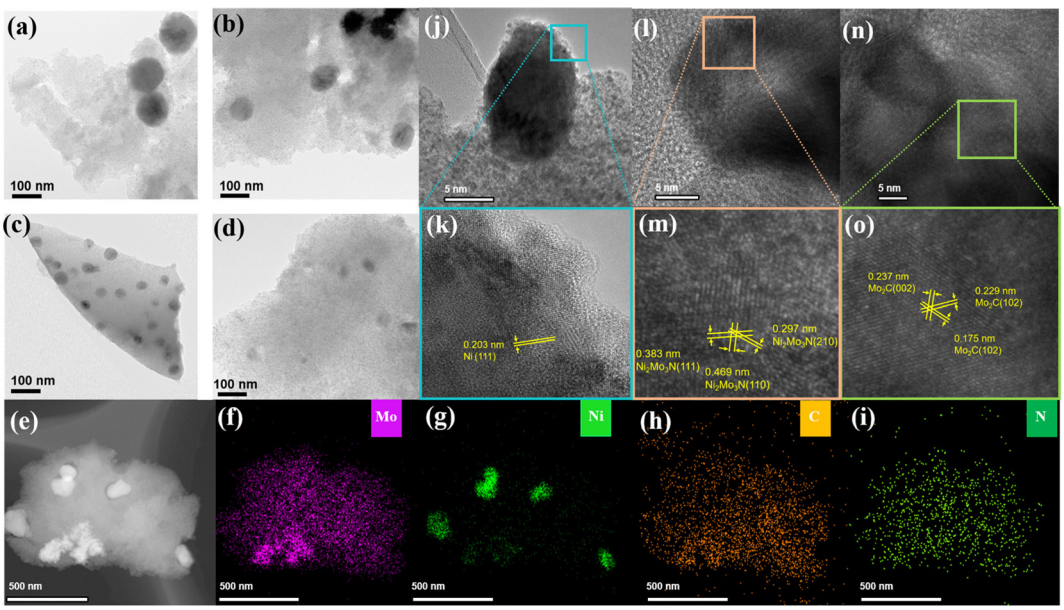

Fig. 3 TEM images of (a) Ni_1Mo_1N/C (b) Ni_1Mo_2N/C (c) Ni_1Mo_3N/C and (d) Ni_1Mo_4N/C catalysts (e–i) EDS elemental mappings and (j–o) HR-TEM images of the Ni_1Mo_3N/C catalyst.

images is representative of the metal particles and the light color region is representative of the C support. The results show that with the increase in Mo addition the particle size became smaller gradually. The Ni_1Mo_3N/C catalyst showed a small metal particle size as well as high dispersion. Although the Ni_1Mo_4N/C catalyst seemed to have the smallest metal particle size the particle dispersion was not uniform which probably had a negative effect on the HDO catalytic performance. The TEM-based EDS examination of Ni_1Mo_3N/C catalysts (Fig. 3e–i) revealed that Ni elements were concentrated inside the particle form whereas the Mo C and N components were evenly dispersed. Furthermore the lattice characteristics of the specific metal phase were examined by HR-TEM. The images in Fig. 3j–m show the lattice characteristics of the (110) (111) and (210) crystal planes of Ni_2Mo_3N and the (111) crystal plane of the metal Ni. Besides lattice fringes belonging to β-Mo_2C were also found in the Ni_1Mo_3N/C catalyst (Fig. 3n and o). These results were in good agreement with the XRD results (Fig. 1).

The valence states of the catalyst components were explored in detail by XPS. The whole spectra of the Ni_xMo_yN/C catalysts are shown in Fig. S7† and the specific element spectra are shown in Fig. 4. As for the Mo 3d spectrum in Fig. 4a the distance between the Mo $3d_{3/2}$ and Mo $3d_{5/2}$ bimodal peaks due to spin–orbit splitting was 3.1 ± 0.3 eV.[32] The signals of the resolved peaks at 229.9 and 232.9 eV were related to Mo^{4+} and Mo^{6+} which were also attributed to the MoO_2 and MoO_3 phases respectively. The fluctuating trend in the content of the above oxide components in these Ni_xMo_yN/C catalysts (Table 2) was consistent with the changes in the oxygen content given in Table 1 which suggests that an increase in the Mo component would result in a greater tendency to produce nitrides or carbides in the Ni_xMo_yN/C catalysts. Furthermore the signal near 228.5 eV in the Ni_1Mo_3N/C and Ni_1Mo_4N/C catalysts was particularly enhanced which points to the presence of Mo^{2+} in the form of Mo–C bonds for the Mo_2C phase.[33] This result was also consistent with the XRD analysis showing the presence of Mo_2C crystals. The binding energy at 228.9 eV was attributed to the $Mo^{\delta+}$ ($0 < \delta < 4$) species which were mainly present in the Ni_2Mo_3N phase.[34,35] In addition a 232.3 eV signal was observed corresponding to the MoO_xC_y phase and assigned to the Mo^{5+} valence state formed by the insertion of oxygen atoms into the carbide lattice of Mo. The undercoordinated Mo^{5+} facilitates the formation of oxygen vacancies and promotes the HDO reaction.[36] Moreover the positions of the Mo deconvolution peaks were also discriminated and the contents of Mo species with different valence states were calculated (Table 2). It was found that the binding energy values of Mo^{2+} $Mo^{\delta+}$ and Mo^{5+} in the Ni_1Mo_3N/C catalysts were shifted to a lower direction compared to the other catalysts. This suggests that the electronic structure of Mo atoms is altered in nitrides and carbides and these negative shifts are related to the down-shift in the d-band center and the high charge density around the Mo species.[37] These results clearly demonstrate the formation of the Ni_2Mo_3N and β-Mo_2C active phase.

Deconvolutional analysis of the Ni 2p spectrum (Fig. 4b) and calculation of the atomic content (Table 2) were also conducted. The results show that Ni^0 and Ni^{2+} valence states were predominantly present in the different Ni_xMo_yN/C catalysts corresponding to binding energies of 852.9 eV and 856.4 eV respectively.[38] The unavoidable Ni surface oxidation resulted in the existence of Ni^{2+} valence states due to the easy oxidation property of Ni metal species. Moreover most the Ni^{2+} component in the Ni_1Mo_3N/C catalyst resulted from the involve-

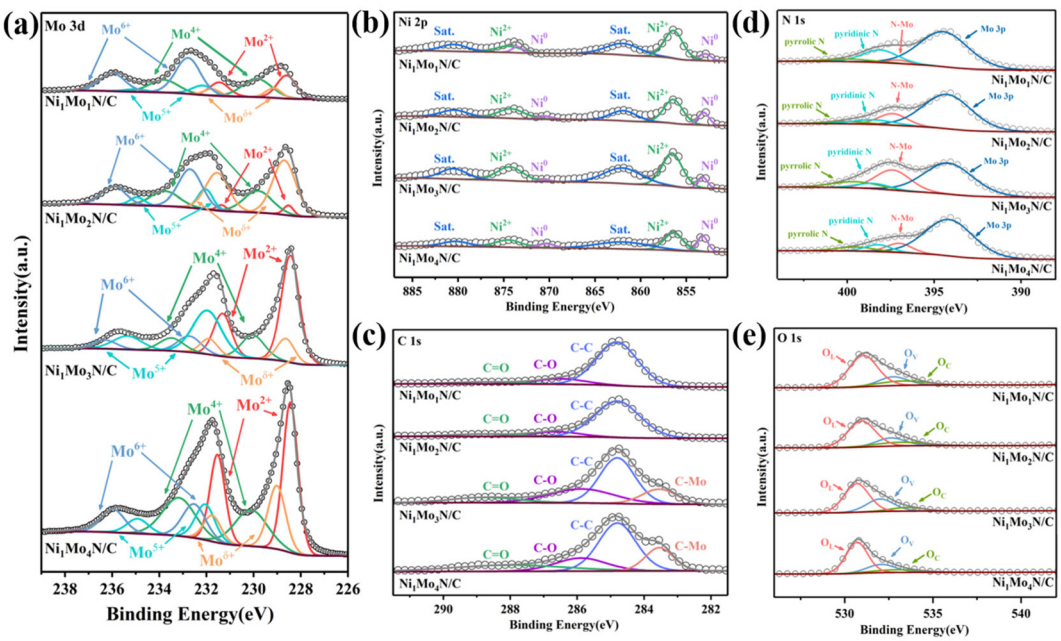

Fig. 4 XPS spectra of Ni_xMo_yN/C catalysts: (a) Mo 3d spectra (b) Ni 2p spectra (c) C 1s spectra (d) N 1s spectra (e) O 1s spectra.

Table 2 Binding energy (eV) and atomic content (%) of Mo and Ni species measured by XPS for the Ni_xMo_yN/C samples

	Mo					Ni	
Samples	Mo^{2+} (Mo_2C)	Mo^{4+} (MoO_2)	$Mo^{\delta+}$ (Ni_2Mo_3N)	Mo^{5+} (MoO_xC_y)	Mo^{6+} (MoO_3)	Ni^0	Ni^{2+} (NiO & Ni_2Mo_3N)
Ni_1Mo_1N/C	228.6 eV (20.3%)	229.9 eV (25.8%)	229.1 eV (7.4%)	232.2 eV (7.7%)	232.8 eV (38.7%)	852.9 eV (17.3%)	856.4 eV (82.7%)
Ni_1Mo_2N/C	228.5 eV (3.2%)	229.8 eV (20.8%)	228.7 eV (41.2%)	232.0 eV (8.3%)	232.7 eV (26.6%)	853.1 eV (20.3%)	856.4 eV (79.7%)
Ni_1Mo_3N/C	228.4 eV (41.8%)	230.0 eV (14.2%)	228.6 eV (10.4%)	232.0 eV (25.5%)	233.5 eV (8.1%)	853.2 eV (10.6%)	856.5 eV (89.4%)
Ni_1Mo_4N/C	228.4 eV (36.2%)	230.1 eV (24.4%)	228.7 eV (10.2%)	232.1 eV (15.9%)	232.5 eV (13.4%)	853.2 eV (30.1%)	856.4 eV (69.9%)

Reaction conditions: 20 mL octane solvent 0.1 g guaiacol 0.05 g catalyst 1 MPa H_2 reaction time was 4 h.

ment of Ni species in the formation of the Ni_2Mo_3N phase which allowed the transformation of Ni^0 to Ni^{2+}.[39] Ni^0 species in Ni_1Mo_3N/C catalyst were observed to have a higher binding energy compared to that in the other catalysts. This shift corresponds to the change in Mo species and led to the moving to a lower binding energy which demonstrates the charge transfer of Ni toward Mo and produces a strong interaction between Ni and Mo. The C 1s peaks of the different Ni_xMo_yN/C catalysts in Fig. 4c could be deconvoluted into three peaks corresponding to C–C (284.8 eV) C–O (286.1 eV) C═O (288.5 eV) respectively.[38] In addition signals attributed to C–Mo bonds were found at 283.7 eV in the cases of the Ni_1Mo_3N/C and Ni_1Mo_4N/C catalysts and indicated the presence of Mo carbides.[33] The XPS spectrum of the N 1s peaks in Fig. 4d showed the presence of pyrrolic N (399.3 eV) and pyridinic N (380.0 eV)[35] indicating that N had been introduced successfully. A peak at a binding energy of 397.2 eV assigned to the N–Mo bond could be observed for all the catalysts while the strongest N–Mo interactions were obtained in the Ni_1Mo_3N/C catalyst.[40] Moreover the strong peak observed near 394.2 eV belonged to the Mo 3p spectrum.[34]

To further investigate the relationship between the undercoordinated Mo^{5+} and oxygen vacancies in the MoO_xC_y phase the O 1s orbital was also analyzed by XPS (Fig. 4e). The deconvolution spectrum at 530.8 eV belonged to lattice oxygen (O_L) which was predominantly present in the oxide phase state of Mo metal. The peak of 532.4 eV belonged to the oxygen vacancies (O_V) and was related to the insertion of lattice carbon into the oxide lattice of Mo to form Mo^{5+} which was capable of a rapid interconversion with Mo^{6+}. Such a redox cycle facilitates the activation of the C–O bond and avoids the hydrogenation of the C═C bond.[37,41,42] Moreover the surface OH groups (O_C) and chemisorbed dissociated oxygen species were associated with the peaks at 533.0–534.2 eV. The content of oxygen vacancies could be estimated by the O_V/O_L ratio. These Ni_xMo_yN/C catalysts had O_V/O_L ratios of 0.28 0.33 0.48 and 0.35 respectively with specified Ni–Mo ratios $x:y$ of 1 : 1 1 : 2 1 : 3 and 1 : 4. These results were consistent with the fluctuation of the Mo^{5+} species. Overall the Ni_1Mo_3N/C catalyst possessed the most oxygen vacancies which would probably facilitate the substrate adsorption and promote the HDO efficiency.

To further characterize the oxygen vacancy property EPR characterization was employed to capture information on the unpaired electrons in different Ni_xMo_yN/C catalysts. As shown in Fig. S8† all the Ni_xMo_yN/C samples had a symmetrical pair of peaks at g = 2.006 which is a typical diagnostic signal for oxygen vacancies. The intensity of the EPR signals was also used to determine the relative content of the oxygen vacancies.[43] Here the Ni_1Mo_3N/C catalyst exhibited the strongest symmetry signal with most electrons trapped in oxygen vacancy sites which was consistent with the XPS results.

In order to explore the hydrogen-adsorption capacity of the catalysts H_2-TPD characterization of the different Ni_xMo_yN/C catalysts was performed. As shown in Fig. 5 compared to the other catalysts the reversible desorption signals of the

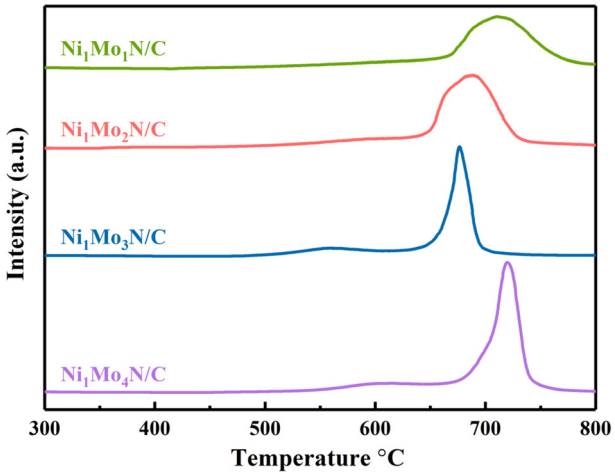

Fig. 5 H_2-TPD profiles of the different Ni_xMo_yN/C catalysts.

Ni_1Mo_3N/C and Ni_1Mo_4N/C catalysts were compressed to a narrow range of desorption temperatures of 650–700 °C and 690–740 °C respectively. This suggests that the active species for the main chemisorption of H_2 had changed. With the increasing Mo the hydrogen-activation species was transformed from metal nickel to bimetallic nitrides and the formed Mo carbide phase also possessed a certain hydrogen-adsorption ability. Besides the doping of N elements into the NiMo alloy lattice resulted in a continuous energy gap around the Fermi level in Ni_2Mo_3N which was associated with a rich metal–ligand structure.[44] Such inherent metallic properties help to accelerate the charge-transfer process and produce adsorption and dissociation effects on hydrogen. In addition Mo_2C was formed as a hexagonal closed packed crystal by the insertion of C atoms while the electron transfer from Mo to C also lowered the electron density surrounding the Mo active site resulting in weak hydrogen bonding and an increased susceptibility to interference with the hydrogen-adsorption process.[45,46] Moreover it has been reported that Mo_2C possesses some Brønsted acidic sites on its surface that have the ability to break C–O bonds in a dehydration process.[47] These complementarities indicate the possibility of a synergy effect between Ni_2Mo_3N and Mo_2C. In addition the H_2 desorption peak of the Ni_1Mo_3N/C catalyst was shifted toward lower temperature compared to that of the Ni_1Mo_4N/C catalyst which demonstrates that desorption of the hydrogen can occur at low temperature and can promote the HDO reaction.

Catalytic HDO of guaiacol and other phenolic compounds

The different Ni_xMo_yN/C catalysts were used for the HDO reaction of guaiacol and the results are shown in Table 3. Guaiacol showed high conversions over Ni_1Mo_2N/C Ni_1Mo_3N/C and Ni_1Mo_4N/C catalysts at 260 °C in which only Ni_1Mo_3N/C presented a complete HDO capability for guaiacol with 95.8% cyclohexane selectivity and 4.2% benzene selectivity. By analyzing the product distribution of these catalysts it was found that the benzene ring of the HDO product over the Ni_1Mo_2N/C catalyst was basically saturated while 38.7% of the benzene ring remained unhydrogenated over the Ni_1Mo_4N/C catalyst. Ni_2Mo_3N and Ni species have a strong ability to activate hydrogen and can be used as metal sites for rapid substrate hydrogenation. With the addition of Mo species the interaction between the Ni and Mo metal was enhanced and a greater Ni_2Mo_3N phase was formed. Besides more β-Mo_2C phase was also generated. Generally β-Mo_2C has a certain direct deoxygenation capacity but little hydrogenation capacity.[45] Therefore under the synergistic catalysis of the Ni_2Mo_3N and β-Mo_2C phase the direct deoxygenation and the hydrogenation–deoxygenation reaction pathways were both promoted thus improving the HDO efficiency significantly. The catalytic results for Ni_1N/C Mo_3N/C and Ni_1Mo_3/C were also compared and it could be found that the Ni_1/C catalyst displayed an insufficient catalytic deoxygenation ability. The absence of a sufficient hydrogen-activation capacity of the Mo_3N/C catalyst led to its poor hydrogenation effect. Although the Ni_1Mo_3/C catalyst displayed the catalytic hydrogenation and deoxygenation effect at the same time its performance was not as effective as that of the Ni_1Mo_3N/C catalyst. Combined with the analysis of the XRD results these experimental results suggest that the active phases of the Ni_2Mo_3N and β-Mo_2C species were responsible for the superior HDO performance of the Ni_1Mo_3N/C catalyst.

Table 3 HDO performance of guaiacol over different catalysts

Catalysts	Conversion (%)	Temperature (°C)	Product selectivity (%)					
					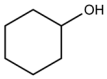	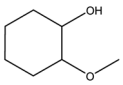	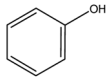	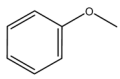
Ni_1Mo_1N/C	7.9	260	8.8	8.1	3.9	—	79.2	—
Ni_1Mo_2N/C	87.1	260	16.2	1.7	56.2	25.2	0.8	—
Ni_1Mo_3N/C	99.9	260	95.8	4.2	—	—	—	—
Ni_1Mo_4N/C	93.0	260	33.8	13.1	27.6	—	17.6	8.0
Ni_1/C	91.2	260	11.5	1.3	48.0	38.6	0.6	—
Mo_3/C	24.3	260	—	—	—	—	99.9	—
Ni_1Mo_3/C	99.9	260	17.7	—	57.6	24.7	—	—
Ni_1Mo_3N/C	53.2	240	14.6	4.0	58.6	15.6	7.2	—
Ni_1Mo_3N/C	38.4	220	7.0	—	47.3	44.0	1.6	—

Combined with the XPS and EPR analysis it could be found that the variation of the Mo^{5+} species content in these Ni_xMo_yN/C catalysts was consistent with the variation in their oxygen vacancy content as well as their HDO performances. Mo^{5+} species are easily oxidized by carbon-containing substrates to the higher valence Mo^{6+} phase thus easily adsorbing the surrounding oxygen-containing substrates with reducing properties.[37] In addition the stronger interactions between Ni and Mo in the Ni_1Mo_3N/C catalyst resulted in a higher charge density around the Mo atoms and the stronger metallicity of Mo species also contributed to a higher efficiency of the catalyst.[38] Besides there was also a small amount of Ni^0 which also plays a role in the H_2-activation procedure. However this is different from the conventional metal–acid site HDO catalytic process. In the absence of significant acid sites the Ni_1Mo_3N/C catalyst still exhibited good HDO performance indicating that Ni_1Mo_3N/C does not completely rely on acid sites to catalyze the conversion of guaiacol to cyclohexane. The combination of hydrogenation deoxygenation and hydrogenolysis finally resulted in a high HDO efficiency of guaiacol. Overall the addition of Mo to the Ni_1Mo_3N/C catalyst contributed to the destruction of the initial carbonaceous structure leading to a decrease in the specific surface area and pore size. While the increased contact between Ni and Mo causes Mo oxides to change into carbide and bimetallic nitride phases. This formation enhances the interaction between Ni and Mo and increases the content of Mo^{5+} simultaneously thus achieving a high HDO activity. Eventually there is a synergistic catalytic effect between the Ni_2Mo_3N phase and β-Mo_2C phase with remarkable lattice features each of which plays a specific catalytic role for a particular reaction step. Due to these factors the Ni_1Mo_3N/C catalyst could display high HDO activity even in the absence of acid conditions.

Given that the HDO performance of the catalysts is highly related to the reaction temperature the influence of the reaction temperature on guaiacol HDO was examined with the Ni_1Mo_3N/C catalyst. As can be seen in the Table 3 relatively few cyclohexane products were produced at a reaction temperature of 220 °C and the conversion of guaiacol was only 38.4%. The conversion rose to 53.2% when the reaction temperature was increased to 240 °C although the selectivity for methoxy cyclohexanol dramatically decreased. This result suggests a considerable elimination of the oxygen-containing functional groups. Also both the conversion and the selectivity of the cyclohexane product rose to about 100% when the reaction temperature was raised to 260 °C. This indicates that increasing the reaction temperature can result in the complete deoxygenation products and that the reaction temperature plays a significant role in the HDO process.

A comparison between the Ni_1Mo_3N/C catalyst in this work and the reported catalysts with acid-free supports was also conducted. Non-precious metals Ni and Co are frequently combined with other active species (such as phosphorus Fe metal and molybdenum carbide) to create HDO catalysts for lignin-derived phenolic compounds. Also the catalytic hydrogenation is commonly carried out at temperatures above 300 °C to achieve high conversion rates (Table 4 entries 2–5). The requirement for high temperature puts high demands on the reactor equipment. The metal Ni has also been used by researchers to couple with molybdenum carbide to design catalysts for the HDO reaction. This kind of catalyst typically needs a higher initial hydrogen pressure to promote C=C saturation which results in a wastage of energy and incurs potential risks (Table 4 entries 6–9). In the studies of the HDO of non-precious metal Co the production of fuel-grade products was difficult to achieve due to its lack of deoxygenation capacity (Table 4 entries 10 and 11) but it may play a role in partial HDO for the production of oxygenated chemicals. Carbides and sulfides of Mo metal as well as carbides of W

Table 4 Comparison of the HDO performances of lignin-derived substrates with various catalysts

Entry	Catalyst	Substrate	T (°C)	Atmosphere condition	Conversion (%)	Hydrocarbon product selectivity (%)	Hydrocarbon product yield (%)
1	Ni_1Mo_3N/C (this work)	Guaiacol	260	1 MPa H_2	99.9	99.9	—
2	Ni/ZrP[48]	Guaiacol	300	4 MPa H_2	100.0	—	80.0
3	Ni–Fe/CNT[49]	Guaiacol	300	3 MPa H_2	<99.0.	<90.0	—
4	$NiMoS_2$/CMK-3[50]	Guaiacol	300	5 MPa H_2	100.0	<60.0	—
5	Ni–P-5-300[51]	*p*-Cresol	350	4 MPa H_2	85.0	65.8	—
6	Ni/β-Mo_2C[52]	Dihydroeugenol	260	2 MPa H_2	100.0	55.0	—
7	Ni_1/β-Mo_2C[52]	25-Dimethoxyphenol	260	4 MPa H_2	100.0	<99.6	—
8	Ni_1/β-Mo_2C[52]	Catechol	260	4 MPa H_2	100.0	<99.9	—
9	Ni–MoC-800[53]	Guaiacol	320	4 MPa H_2	73.2	2.6	—
10	Co/ZrP[48]	Guaiacol	300	7 MPa H_2	100.0	—	76.0
11	Co–Mo-0.5-200[54]	*p*-Cresol	275	4 MPa H_2	100.0	6.3	—
12	Mo_2C/CNF[55]	Guaiacol	300	2 Mpa H_2	67.0	11.1	—
13	Mo_2C/CNF[56]	Guaiacol	300	2 MPa H_2	79.7	—	60.0
14	Mo_2C@C[57]	Guaiacol	340	2.8 MPa H_2	76.3	—	0
15	Mo_2C/CNF[58]	Guaiacol	300	2 MPa H_2	<99.0	—	<42.7
16	MoS_2/AC[59]	Eugenol	300	3 MPa H_2	99.9	—	4.2
17	MoS_2/C[60]	Guaiacol	300	5 MPa H_2	86.0	—	<10.0
18	W_2C/CNF[61]	Guaiacol	350	5.5 MPa H_2	66.0	<2.0	—
19	RuO_2–ZM[62]	Guaiacol	300	2 MPa H_2	<70.0	—	<10.0
20	MoO_3/AC[59]	Eugenol	300	3 MPa H_2	74.6	—	0

have also been used to conduct the HDO of lignin-derived phenolic compounds. Molybdenum carbide species have a certain hydrogenolysis capacity but due to the insufficiency of their hydrogen activation the combination of them with components with a strong hydrogen-activation capacity may be an effective solution to improve their HDO capacity (Table 4 entries 12–15). Mo sulfide species are traditionally used as catalysts for fossil energy improvements but it is difficult to maintain their stability due to the gradual loss of their S elements during the reaction (Table 4 entries 16 and 17). Also the gradual popularization of S-free renewable fuels today signals resistance to the widespread usage of S-containing catalysts. W_2C has also been used in HDO for the upgrading of biomass fractions to fuels due to the fact that W has a configuration of an extra-nuclear electron similar to that of Mo (Table 4 entry 18). However its performance seems to be inferior to that of the active Mo-based catalysts even under more adequate reaction conditions. Metal oxides have also been used as HDO catalysts for the upgrading of phenolic compounds (Table 4 entries 19 and 20) but their performances are limited and need further development. Overall in comparison to other reported works using different Ni-based catalysts and Mo-based catalysts without acid addition the results in this work were far superior in terms of the mild reaction conditions and high hydrocarbon product selectivity.

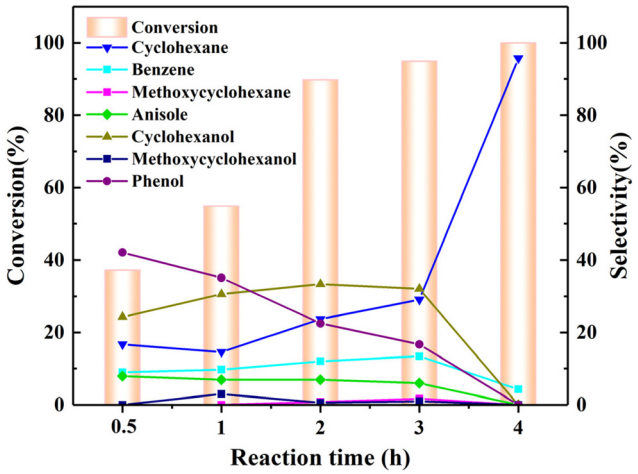

Fig. 6 Results of varying the reaction time on the HDO of guaiacol. Conditions: 0.1 g guaiacol 0.05 g Ni_1Mo_3N/C 20 mL octane 260 °C 1 MPa H_2 4 h.

To reveal the HDO reaction pathway of guaiacol the effect of the reaction time on the real-time product distribution was also investigated. As shown in Fig. 6 the conversion of guaiacol could reach 89.9% after 2 h of reaction and the selectivities for cyclohexane benzene methoxycyclohexanol and cyclohexanol were 23.7% 12.0% 33.4% and 22.5% respectively. The selectivity of cyclohexane increased to 95.8% when the reaction time was increased to 4 h. Remarkably the products from the reaction time of 0.5 h showed a distribution of 42.1% phenol and 7.9% anisole. This implies that a portion of the guaiacol is first dehydroxylated or methoxylated prior to hydrogenation during the reaction. This pathway is different from common studies which typically take into account hydrogenation of the benzene ring of lignin-derived phenolic compounds at the

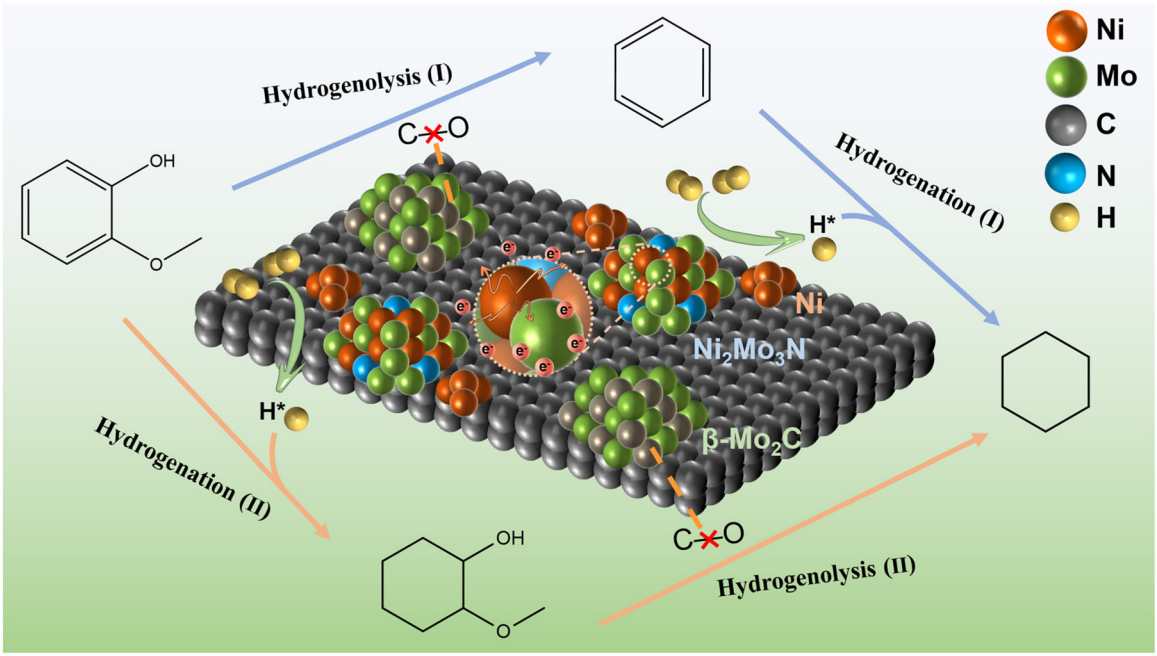

Fig. 7 Schematic illustration showing the catalytic role of the multiple active components in the catalysts and the possible HDO pathways of guaiacol over Ni_1Mo_3N/C catalyst.

metallicity site into a saturated product as a favorable condition for the deoxygenation reaction during the operation of a bifunctional metal–acid multiphase catalyst.[15] Moreover the selectivity for methoxy cyclohexane and methoxy cyclohexanol products remains low most likely due to their roles as chemical intermediates that may be quickly converted to cyclohexane and cyclohexanol respectively. Based on the real-time product distributions the possible reaction pathways were identified. As shown in Fig. 7 there are two different reaction pathways. (1) Guaiacol is first successively deoxygenated at the β-Mo_2C site to produce an unsaturated benzene ring without oxygen followed by hydrogenation at the Ni_2Mo_3N site and Ni site to produce a cyclohexane product; (2) guaiacol first saturates the benzene ring with activated hydrogen at the Ni_2Mo_3N site and Ni site and then dehydrates at the β-Mo_2C site to form a fully deoxygenated cyclohexane. These two reaction pathways display a competitive relation thus resulting in the formation of benzene and methoxycyclohexanol as the intermediate products respectively.

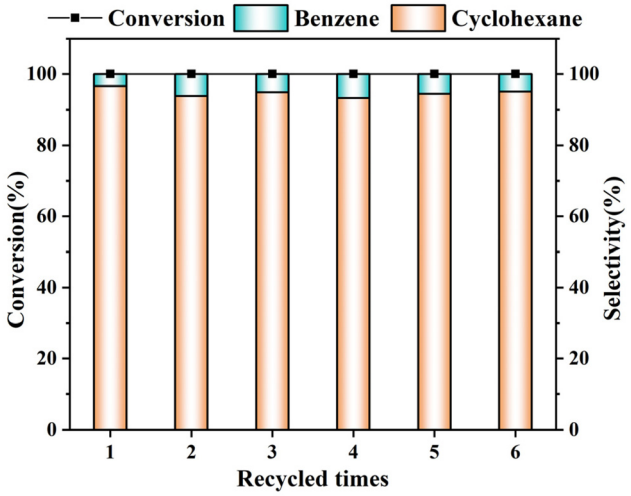

Fig. 8 Results for the catalyst recycling times on the HDO of guaiacol. Conditions: 0.1 g guaiacol 0.05 g Ni_1Mo_3N/C 20 mL octane 260 °C 1 MPa H_2 4 h.

To further investigate the reusability of the Ni_1Mo_3N/C catalyst recycling tests were also conducted. The recycled catalyst was washed with deionized water and ethanol after each reaction and the subsequent recycle reaction was then carried out under the same parameters as previously mentioned. As can be seen in Fig. 8 the catalyst exhibited high recycle stability even after six consecutive operations maintaining 99.9% conversion and 99.9% hydrocarbons selectivity (benzene and

Table 5 Catalytic HDO of other phenolic model compounds derived from lignin

Substrates	Conversion (%)	Selectivity (%)		
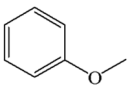	99.9	 97.8	 2.2	—
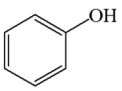	99.9	 97.2	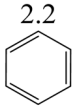 2.8	—
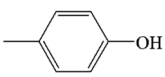	99.9	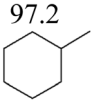 95.5	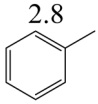 4.5	—
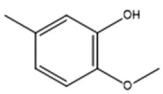	99.9	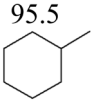 90.2	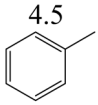 9.8	—
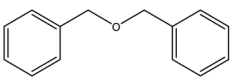	99.9	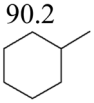 46.0	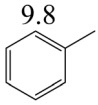 54.0	—
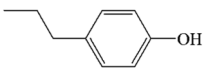	99.9	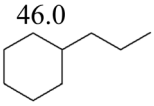 88.9	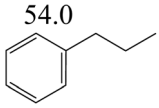 11.1	—
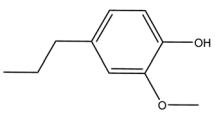	99.9	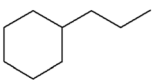 84.6	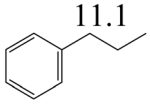 10.6	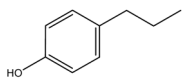 4.8

Conditions: 0.1 g model compounds 0.05 g Ni_1Mo_3N/C 20 mL octane 260 °C 1 MPa H_2 4 h.

cyclohexane). These results demonstrate the high stability of the Ni_1Mo_3N/C catalyst which presents it with great potential for practical application in the HDO upgrade of lignin-derived phenolic compounds.

Catalytic HDO of other phenolic model compounds and raw lignin oil

Other model phenolic compounds derived from lignin (including anisole phenol *p*-cresol dibenzyl ether 4-propylphenol and 2-methoxy-4-(1-propyl) phenol) were also tested for their HDO properties as substrates according to the screened reaction conditions. As shown in Table 5 the Ni_1Mo_3N/C catalyst performed well in the HDO reaction of most phenolic compounds. Among them nearly all of the oxygen-containing functional groups were eliminated including anisole phenol *p*-cresol dibenzyl ether and 4-propylphenol. Even though it was not totally deoxygenated 2-methoxy-4-(1-propyl) phenol also produced 95.2% of the total alkane yield. Notably following the HDO procedure unsaturated benzene-ringed hydrocarbons were also found in the HDO products of these lignin-derived phenolic compounds. Particularly with dibenzyl ether as a substrate 54.0% toluene selectivity was achieved. This suggests that in the HDO reaction of the Ni_1Mo_3N/C catalyst the process of dehydration of the benzene ring followed by hydrogenation to form alkanes may include a rate-determining step in the total reaction leaving the benzene ring not yet fully saturated. Also the presence of *p*-propyl phenol after the HDO process for 2-methoxy-4-(1-propyl) phenol indicates that the ether bond on the benzene ring could be more easily broken than the hydroxyl group during the hydrogenolysis process over the β-Mo_2C site. The steric effect may be responsible for the incomplete deoxygenation effect due to the growth of the carbon chains of the substrate molecules.[63]

Owing to the high concentration of unsaturated bonds and oxygen-containing groups raw lignin oil is rarely directly used as a liquid fuel until it has been refined and upgraded by an HDO approach. The Ni_1Mo_3N/C catalyst was also investigated to examine its HDO characteristics for the lignin oil composite fractions. Table 6 and Fig. S9† display the precise composition of the lignin oil both before and after HDO upgrading. Analysis of the raw lignin oil indicates that it consisted of 5.7% hydrocarbons 19.0% alkylphenols and 74.4% guaiacols and syringols and 0.9% other oxygenated compounds. The stability and calorific value of lignin oil were significantly increased by HDO modification at 260 °C. The guaiacols and syringols components completely disappeared with the hydrocarbon content increasing to 88.4%. The hydrocarbon products included a certain amount of arenes and their content reached 18.2% which was similar to the results for the HDO of other model compounds. This result is quite different from other reported

Table 6 Components of the raw lignin oil and upgraded lignin oil at 260 °C as analyzed by GC-MS

Raw lignin oil			Upgraded lignin oil		
RT (min)	Component	Content (%)	RT (min)	Component	Content (%)
Hydrocarbons		**5.7**	**Hydrocarbons**		**88.4**
22.92	3-Methylphenylacetylene	1.5	1.72	Cyclohexane	22.9
26.05	Naphthalene	3.2	2.51	Cyclohexane 13-dimethyl-	14.0
27.30	Naphthalene 2-methyl-	0.9	2.84	Cyclohexane ethyl-	9.0
Alkylphenols		**19.0**	3.59	Benzene	0.7
27.38	Phenol 26-dimethyl-	1.0	4.37	Cyclohexane propyl-	19.4
28.04	Phenol 3-methyl-	8.7	6.16	Toluene	3.1
28.58	*p*-Cresol	8.4	7.51	Cyclohexane butyl-	1.2
29.24	Phenol 3-ethyl-	1.0	9.49	Ethylbenzene	3.1
Guaiacols and syringols		**74.4**	13.06	Benzene propyl-	2.4
27.01	Phenol 2-methoxy-	19.8	19.99	Indane	1.8
27.09	Phenol 2-methoxy-5-methyl-	1.7	22.73	Benzene 1-methyl-4-(2-propenyl)-	0.9
28.79	Phenol 2-methoxy-4-propyl-	5.1	23.17	Benzene 2-ethenyl-14-dimethyl-	1.1
29.11	Phenol 2-ethyl-6-methyl-	1.3	23.56	Naphthalene 1234-tetrahydro-	2.7
29.19	Eugenol	9.1	24.92	Naphthalene 1234-tetrahydro-6-methyl-	1.1
29.50	26-Dimethoxytoluene	1.3	25.30	Benzene cyclohexyl-	1.0
29.73	Phenol 2-methoxy-4-(1-propenyl)-	6.6	**Alkylphenols**		**9.8**
29.78	Phenol 26-dimethoxy-	5.1	24.66	Phenol 3-methyl-6-propyl-	1.7
30.30	Phenol 2-methoxy-4-(1-propenyl)-(Z)-	18.4	27.38	Phenol 26-dimethyl-	0.7
30.62	Benzene 123-trimethoxy-5-methyl-	2.7	28.04	Phenol 3-methyl-	1.9
31.43	Phenol 26-dimethoxy-4-(2-propenyl)-	2.0	28.50	Phenol 3-ethyl-	0.4
32.00	(*E*)-26-Dimethoxy-4-(prop-1-en-1-yl)phenol	1.2	28.57	Phenol 23-dimethyl-	2.4
Other oxygenated compounds		**0.9**	29.63	2-Methyl-6-propylphenol	0.7
25.16	Acetophenone	0.9	29.76	Phenol 2-propyl-	1.1
			Guaiacols and syringols		**0**
			Other oxygenated compounds		**1.8**
			22.27	Benzene 1-methoxy-3-methyl-	0.9
			23.65	3-Ethylphenol methyl ether	0.9

Conditions: 0.05 g Ni_1Mo_3N/C 3 g raw lignin oil extracted by 20 mL octane 1 MPa H_2 260 °C 4 h. The content was calculated by the peak areas. Components listed are those represented for more than 0.4% of the content. RT: retention time.

studies since the removal of oxygen from lignin oil is often accompanied by a process of benzene ring saturation due to the consumption of large amounts of hydrogen and the existence of strong acid sites.[64,65] Overall the novel Ni_1Mo_3N/C catalyst in this work has the potential to provide new pathways to convert lignin oil into high-quality liquid biofuels.

Conclusion

In this study a series of Ni_xMo_yN/C catalysts with different Ni and Mo molar ratios were fabricated without the addition of acid sites and were employed for the HDO of lignin-derived phenolic compounds. The Ni_1Mo_3N/C catalyst exhibited outstanding HDO performance which involved hydrogenation deoxygenation and hydrogenolysis at the same time. The efficient hydrogen activation as well as the cleavage of C–O bonds could be achieved under the synergic catalysis of Ni Ni_2Mo_3N and β-Mo_2C. The strong interaction between Ni and Mo favored the dispersion of Ni and Ni_2Mo_3N which significantly promoted the HDO activity. With a 95.8% cyclohexane selectivity guaiacol was completely converted at 260 °C and the benzene by-product was also obtained as a valuable fuel additive. The Ni_1Mo_3N/C catalyst also presented high stability without activity loss after six cyclic runs. In addition raw lignin oil was upgraded through the HDO reaction using the Ni_1Mo_3N/C catalyst. The hydrocarbon content increased from 5.7% to 88.4% and the arenes accounted for 18.2% of the hydrocarbon products due to the presence of a hydrogenolysis reaction pathway which presents potential for the direct production of hydrocarbon liquid biofuels containing aromatic fuel additives. This catalytic system shows great potential for the conversion of lignin oil into high-quality hydrocarbon liquid fuels. We hope this paper provides valuable insights for the development of catalytic lignin conversion processes and for the field of green chemistry.

Data availability

Data sharing is not applicable to this article as no new data were created or analyzed in this study. The data that supports the findings of this study are available in the ESI† of this article.

Conflicts of interest

There are no conflicts to declare.

Acknowledgements

The authors acknowledge the Young Elite Scientists Sponsorship Program by CAST (2022QNRC001) National Natural Science Foundation of China (No. 22278088) Guangdong Natural Science Foundation (No. 2023A1515030159) and Open Project of Yunnan Precious Metals Laboratory Co. Ltd (No. YPML-2023050261) for their financial supports of this work. We would like to thank Analysis and Test Center of Guangdong University of Technology for the EPR analysis.

References

1 B. Jiang, L. Li, Z. Bian, Z. Li, M. Othman, Z. Sun, D. Tang, S. Kawi and B. Dou, Hydrogen generation from chemical looping reforming of glycerol by Ce-doped nickel phyllosilicate nanotube oxygen carriers, *Fuel*, 2018, **222**, 185–192.
2 R. Zhang, J. Zhang, H. Liu, Z. Jiang, X. Liu, W. Wang, L. Peng and C. Hu, Toward Value-Added Chemicals from Carbohydrates via C–C Bond Cleavage and Coupling Transformations, *ACS Catal.*, 2024, **14**, 5167–5197.
3 S. S. Wong, R. Shu, J. Zhang, H. Liu and N. Yan, Downstream processing of lignin derived feedstock into end products, *Chem. Soc. Rev.*, 2020, **49**, 5510–5560.
4 Z. Xiong, J. Guo, W. Chaiwat, W. Deng, X. Hu, H. Han, Y. Chen, K. Xu, S. Su, S. Hu, Y. Wang and J. Xiang, Assessing the chemical composition of heavy components in bio-oils from the pyrolysis of cellulose hemicellulose and lignin at slow and fast heating rates, *Fuel Process. Technol.*, 2020, **199**, 106299.
5 S. Gillet, M. Aguedo, L. Petitjean, A. R. C. Morais, A. M. da Costa Lopes, R. M. Łukasik and P. T. Anastas, Lignin transformations for high value applications: towards targeted modifications using green chemistry, *Green Chem.*, 2017, **19**, 4200–4233.
6 S. Yang, G. Chen, Q. Guan, H. Xu, Z. Wang, B. Liu, S. Yang, T. Lei, X. Zeng and L. Lin, An efficient Pd/carbon-silica-alumina catalyst for the hydrodeoxygenation of bio-oil model compound phenol, *Mol. Catal.*, 2021, **510**, 111681.
7 S. Oh, J. H. Lee and J. W. Choi, Hydrodeoxygenation of crude bio-oil with various metal catalysts in a continuous-flow reactor and evaluation of emulsion properties of upgraded bio-oil with petroleum fuel, *Renewable Energy*, 2020, **160**, 1160–1167.
8 R. Li, J. Qiu, H. Chen, R. Shu, Y. Chen, Y. Liu and P.-F. Liu, Hydrodeoxygenation of phenolic compounds and raw lignin-oil over bimetallic RuNi catalyst: An experimental and modeling study focusing on adsorption properties, *Fuel*, 2020, **281**, 118758.
9 Z. He, M. Hu and X. Wang, Highly effective hydrodeoxygenation of guaiacol on Pt/TiO_2: Promoter effects, *Catal. Today*, 2018, **302**, 136–145.
10 L. Nie and D. E. Resasco, Kinetics and mechanism of m-cresol hydrodeoxygenation on a Pt/SiO_2 catalyst, *J. Catal.*, 2014, **317**, 22–29.
11 C. Chen, X. Ji, Y. Xiong and J. Jiang, Environmentally-friendly preparation of natural hollow carbon spheres derived from a biomass puffball for in situ upgrading of lignin-derived vanillin, *Green Chem.*, 2024, **26**, 1488–1500.

12 D. R. Stellwagen and J. H. Bitter, Structure–performance relations of molybdenum- and tungsten carbide catalysts for deoxygenation, *Green Chem.*, 2015, **17**, 582–593.
13 J. Remón, E. Ochoa, C. Foguet, J. L. Pinilla and I. Suelves, Towards a sustainable bio-fuels production from lignocellulosic bio-oils: Influence of operating conditions on the hydrodeoxygenation of guaiacol over a Mo_2C/CNF catalyst, *Fuel Process. Technol.*, 2019, **191**, 111–120.
14 S. Arora, N. Gupta and V. Singh, Improved Pd/Ru metal supported graphene oxide nano-catalysts for hydrodeoxygenation (HDO) of vanillyl alcohol vanillin and lignin, *Green Chem.*, 2020, **22**, 2018–2027.
15 X. Wang, M. Arai, Q. Wu, C. Zhang and F. Zhao, Hydrodeoxygenation of lignin-derived phenolics – a review on the active sites of supported metal catalysts, *Green Chem.*, 2020, **22**, 8140–8168.
16 G. Xu, C. Li, T. Deng, C. Wang, Y. Zhang and Y. Fu, Kinetic Studies on the Impact of Pd Addition to Ru/TiO2 Catalyst: Levulinic Acid to γ-Valerolactone under Ambient Hydrogen Pressure, *Ind. Eng. Chem. Res.*, 2020, **59**, 17279–17286.
17 F.-P. Wu, L.-L. Qiu, Y.-P. Zhao, Z.-P. Fu, J. Xiao, J. Li, F.-J. Liu, J. Liang and J.-P. Cao, Hydrogen source controlled hydrodeoxygenation of phenolic compounds to cycloalkanes/cycloalkanols over NiFeAlOx catalysts, *Fuel Process. Technol.*, 2023, **252**, 107977.
18 Q. Chen, C. Cai, X. Zhang, Q. Zhang, L. Chen, Y. Li, C. Wang and L. Ma, Amorphous FeNi–ZrO_2-Catalyzed Hydrodeoxygenation of Lignin-Derived Phenolic Compounds to Naphthenic Fuel, *ACS Sustainable Chem. Eng.*, 2020, **8**, 9335–9345.
19 W. Wang, L. Li, S. Tan, K. Wu, G. Zhu, Y. Liu, Y. Xu and Y. Yang, Preparation of NiS_2//MoS_2 catalysts by two-step hydrothermal method and their enhanced activity for hydrodeoxygenation of *p*-cresol, *Fuel*, 2016, **179**, 1–9.
20 R. Li, J. Qiu, H. Chen, R. Shu, Y. Chen, Y. Liu and P.-F. Liu, Hydrodeoxygenation of phenolic compounds and raw lignin-oil over bimetallic RuNi catalyst: An experimental and modeling study focusing on adsorption properties, *Fuel*, 2020, **281**, 118758.
21 R. Shu, R. Li, Y. Liu, C. Wang, P.-F. Liu and Y. Chen, Enhanced adsorption properties of bimetallic RuCo catalyst for the hydrodeoxygenation of phenolic compounds and raw lignin-oil, *Chem. Eng. Sci.*, 2020, **227**, 115920.
22 S. Cheng, L. Wei, J. Julson and M. Rabnawaz, Upgrading pyrolysis bio-oil through hydrodeoxygenation (HDO) using non-sulfided Fe-Co/SiO_2 catalyst, *Energy Convers. Manage.*, 2017, **150**, 331–342.
23 C. R. Lee, J. S. Yoon, Y.-W. Suh, J.-W. Choi, J.-M. Ha, D. J. Suh and Y.-K. Park, Catalytic roles of metals and supports on hydrodeoxygenation of lignin monomer guaiacol, *Catal. Commun.*, 2012, **17**, 54–58.
24 M. Saidi, F. Samimi, D. Karimipourfard, T. Nimmanwudipong, B. C. Gates and M. R. Rahimpour, Upgrading of lignin-derived bio-oils by catalytic hydrodeoxygenation, *Energy Environ. Sci.*, 2013, **7**, 103–129.
25 E. Laurent and B. Delmon, Study of the hydrodeoxygenation of carbonyl carboxylic and guaiacyl groups over sulfided CoMo/γ-Al_2O_3 and NiMo/γ-Al_2O_3 catalysts, *Appl. Catal., A*, 1994, **109**, 77–96.
26 S. Echeandia, P. L. Arias, V. L. Barrio, B. Pawelec and J. L. G. Fierro, Synergy effect in the HDO of phenol over Ni–W catalysts supported on active carbon: Effect of tungsten precursors, *Appl. Catal., B*, 2010, **101**, 1–12.
27 S. Ma, L. Zhang, L. Zhu and X. Zhu, Preparation of multipurpose bio-oil from rice husk by pyrolysis and fractional condensation, *J. Anal. Appl. Pyrolysis*, 2018, **131**, 113–119.
28 B. Chen, X. Zheng, J. Gu, S. Qiu, J. Song, X. Wu, H. Dong, Q. Zhang and T. Wang, Engineering Sn doping Ni/chitosan to boost higher alcohols synthesis from direct coupling of aqueous ethanol: Modifying adsorption of aldehyde intermediates for C-C bond cleavage suppressing, *Appl. Catal., B*, 2023, **321**, 122048.
29 X. Chen, X. Chen, J. Wang and C. Liang, Steerable Engineering of Nickel Molybdenum Carbonitride Nanostructures for Catalytic Regioselectivity Cleavage of C–O and C–C Bonds in Deoxygenation of Methyl Palmitate, *ACS Appl. Nano Mater.*, 2022, **5**, 14987–14998.
30 L. Li, C. Chen, X. Chen, X. Zhang, T. Huang and A. Yu, Structure and Catalyst Effects on the Electrochemical Performance of Air Electrodes in Lithium-Oxygen Batteries, *ChemElectroChem*, 2018, **5**, 2666–2671.
31 H. Li, F. Zhen, X. Qian, J. Yang, H. Yu, Q. Wang, L. Zhang, Y. Wang and B. Qu, Study of efficient catalytic electrode for hydrogen evolution reaction from seawater based on low tortuosity corn straw cellulose biochar/Mo_2C with porous channels, *Int. J. Biol. Macromol.*, 2024, **254**, 127993.
32 C. Zhao, J. Wang, X. Chen and C. Liang, Nickel Molybdenum Bimetallic Nitrides as Efficient Catalysts for the Hydrodeoxygenation of Methyl Palmitate, *Eur. J. Inorg. Chem.*, 2023, **26**, e202300073.
33 X. Zan, J. Wang, X. Luo, Z. Wu and L. Ye, In Situ Preparation of Mo 2 C Nanoparticles Embedded in Ketjenblack Carbon as Highly Efficient Electrocatalysts for Hydrogen Evolution, *ACS Sustainable Chem. Eng.*, 2018, **6**(1), 983–990.
34 M. Hou, R. Lan, Z. Hu and Z. Chen, The preparation of Ni/Mo-based ternary electrocatalysts by the self-propagating initiated nitridation reaction and their application for efficient hydrogen production, *Nanoscale*, 2019, **11**, 17093–17103.
35 H. Yan, Y. Xie, Y. Jiao, A. Wu, C. Tian, X. Zhang, L. Wang and H. Fu, Holey Reduced Graphene Oxide Coupled with an Mo2N–Mo2C Heterojunction for Efficient Hydrogen Evolution, *Adv. Mater.*, 2018, **30**, 1704156.
36 H. Wang, S. Liu and K. J. Smith, Synthesis and Hydrodeoxygenation Activity of Carbon Supported Molybdenum Carbide and Oxycarbide Catalysts, *Energy Fuels*, 2016, **30**, 6039–6049.
37 K. Murugappan, E. M. Anderson, D. Teschner, T. E. Jones, K. Skorupska and Y. Román-Leshkov, Operando NAP-XPS unveils differences in MoO_3 and Mo_2C during hydrodeoxygenation, *Nat. Catal.*, 2018, **1**, 960–967.

38 J. Liao, Z. Liu, Y. Ling, Q. Zhang, S. Qiu, J. Gu, J. Li, H. Dong, J. Song and T. Wang, Electronic and surface engineering of Mo doped Ni@C nanocomposite boosting catalytic upgrading of aqueous bio-ethanol to bio-jet fuel precursors, *Chem. Eng. J.*, 2023, **461**, 141888.
39 X. Du, X. Lei, L. Zhou, Y. Peng, Y. Zeng, H. Yang, D. Li, C. Hu and H. Garcia, Bimetallic Ni and Mo Nitride as an Efficient Catalyst for Hydrodeoxygenation of Palmitic Acid, *ACS Catal.*, 2022, **12**, 4333–4343.
40 W.-F. Chen, K. Sasaki, C. Ma, A. I. Frenkel, N. Marinkovic, J. T. Muckerman, Y. Zhu and R. R. Adzic, Hydrogen-Evolution Catalysts Based on Non-Noble Metal Nickel–Molybdenum Nitride Nanosheets, *Angew. Chem., Int. Ed.*, 2012, **51**, 6131–6135.
41 M. Rellán-Piñeiro and N. López, One Oxygen Vacancy Two Charge States: Characterization of Reduced α-MoO_3(010) through Theoretical Methods, *J. Phys. Chem. Lett.*, 2018, **9**, 2568–2573.
42 C. Yu, S. Yu and L. Li, Upgraded methyl oleate to diesel-like hydrocarbons through selective hydrodeoxygenation over Mo-based catalyst, *Fuel*, 2022, **308**, 122038.
43 G. Li, K. He, F. Zhang, G. Jiang, Z. Zhao, Z. Zhang, J. Cheng and Z. Hao, Defect enhanced CoMnNiOx catalysts derived from spent ternary lithium-ion batteries for low-temperature propane oxidation, *Appl. Catal., B*, 2022, **309**, 121231.
44 J. Y. Zhao, Z. X. Lou, L. Y. Xue, Y. Ding, X. Li, X. Wu, Y. Liu, H. Y. Yuan, H. F. Wang, P. F. Liu, S. Dai and H. G. Yang, Rational nitrogen alloying in nickel–molybdenum nitride can mediate efficient and durable alkaline hydrogen evolution, *J. Mater. Chem. A*, 2023, **11**, 7256–7263.
45 X. Zhang, T. Liu, T. Guo, Z. Mu, X. Hu, K. He, X. Chen, V. P. Dravid, Z. Wu and D. Wang, High-Performance MoC Electrocatalyst for Hydrogen Evolution Reaction Enabled by Surface Sulfur Substitution, *ACS Appl. Mater. Interfaces*, 2021, **13**, 40705–40712.
46 S. Jiang, X. Wu, X. Liu, W. Ma, J. Song, R. Shu, Q. Zhang and S. Qiu, Molybdenum Carbide for Catalytic De/hydrogenation Process: Synthesis Modulation and Applications, *ChemCatChem*, 2023, **15**, e202300798.
47 M. M. Sullivan and A. Bhan, Acetone Hydrodeoxygenation over Bifunctional Metallic–Acidic Molybdenum Carbide Catalysts, *ACS Catal.*, 2016, **6**, 1145–1152.
48 G.-H. Han, M. W. Lee, S. Park, H. J. Kim, J.-P. Ahn, M. Seo and K.-Y. Lee, Revealing the factors determining the selectivity of guaiacol HDO reaction pathways using ZrP-supported Co and Ni catalysts, *J. Catal.*, 2019, **377**, 343–357.
49 H. Fang, J. Zheng, X. Luo, J. Du, A. Roldan, S. Leoni and Y. Yuan, Product tunable behavior of carbon nanotubes-supported Ni–Fe catalysts for guaiacol hydrodeoxygenation, *Appl. Catal., A*, 2017, **529**, 20–31.
50 S. Mukundan, M. A. Wahab, L. Atanda, M. Konarova and J. Beltramini, Highly active and robust Ni–MoS_2 supported on mesoporous carbon: a nanocatalyst for hydrodeoxygenation reactions, *RSC Adv.*, 2019, **9**, 17194–17202.
51 W. Wang, K. Zhang, H. Liu, Z. Qiao, Y. Yang and K. Ren, Hydrodeoxygenation of p-cresol on unsupported Ni–P catalysts prepared by thermal decomposition method, *Catal. Commun.*, 2013, **41**, 41–46.
52 H. Guo, J. Zhao, Y. Chen, X. Lu, Y. Yang, C. Ding, L. Wu, L. Tan, J. Long, G. Yang, Y. Tang, N. Tsubaki and X. Gu, Mechanistic Insights into Hydrodeoxygenation of Lignin Derivatives over Ni Single Atoms Supported on Mo_2C, *ACS Catal.*, 2024, **14**, 703–717.
53 A. V. Vasilevich, O. N. Baklanova and A. V. Lavrenov, Hydrodeoxygenation of Guaiacol with Molybdenum-Carbide-Based Carbon Catalysts, *ChemistrySelect*, 2020, **5**, 4575–4579.
54 W. Wang, K. Zhang, L. Li, K. Wu, P. Liu and Y. Yang, Synthesis of Highly Active Co–Mo–S Unsupported Catalysts by a One-Step Hydrothermal Method for p-Cresol Hydrodeoxygenation, *Ind. Eng. Chem. Res.*, 2014, **53**, 19001–19009.
55 E. Ochoa, D. Torres, J. L. Pinilla and I. Suelves, Nanostructured Carbon Material Effect on the Synthesis of Carbon-Supported Molybdenum Carbide Catalysts for Guaiacol Hydrodeoxygenation, *Energies*, 2020, **13**, 1189.
56 E. Ochoa, D. Torres, J. L. Pinilla and I. Suelves, Influence of carburization time on the activity of Mo_2C/CNF catalysts for the HDO of guaiacol, *Catal. Today*, 2020, **357**, 240–247.
57 R. Li, A. Shahbazi, L. Wang, B. Zhang, A. M. Hung and D. C. Dayton, Graphite encapsulated molybdenum carbide core/shell nanocomposite for highly selective conversion of guaiacol to phenolic compounds in methanol, *Appl. Catal., A*, 2016, **528**, 123–130.
58 E. Ochoa, D. Torres, J. L. Pinilla and I. Suelves, On the hydrothermal-enhanced synthesis of highly selective Mo_2C catalysts to fully deoxygenated products in the guaiacol HDO reaction, *J. Environ. Chem. Eng.*, 2021, **9**, 105146.
59 N. Ji, X. Diao, X. Li, Z. Jia, Y. Zhao, X. Lu, C. Song, Q. Liu and C. Li, Toward Alkylphenols Production: Lignin Depolymerization Coupling with Methoxy Removal over Supported MoS_2 Catalyst, *Ind. Eng. Chem. Res.*, 2020, **59**, 17287–17299.
60 S. Mukundan, M. Konarova, L. Atanda, Q. Ma and J. Beltramini, Guaiacol hydrodeoxygenation reaction catalyzed by highly dispersed single layered MoS_2/C, *Catal. Sci. Technol.*, 2015, **5**, 4422–4432.
61 A. L. Jongerius, R. W. Gosselink, J. Dijkstra, J. H. Bitter, P. C. A. Bruijnincx and B. M. Weckhuysen, Carbon Nanofiber Supported Transition-Metal Carbide Catalysts for the Hydrodeoxygenation of Guaiacol, *ChemCatChem*, 2013, **5**, 2964–2972.
62 E. R. Naranov, A. A. Sadovnikov, O. V. Arapova, A. L. Bugaev, O. A. Usoltsev, D. N. Gorbunov, V. Russo, D. Y. Murzin and A. L. Maximov, Mechanistic insights on Ru nanoparticle in situ formation during hydrodeoxygenation of lignin-derived substances to hydrocarbons, *Catal. Sci. Technol.*, 2023, **13**, 1571–1583.
63 J. Zhang, L. Wang, Y. Shao, Y. Wang, B. C. Gates and F.-S. Xiao, A Pd@Zeolite Catalyst for Nitroarene

Hydrogenation with High Product Selectivity by Sterically Controlled Adsorption in the Zeolite Micropores, *Angew. Chem., Int. Ed.*, 2017, **56**, 9747–9751.

64 R. Shu, H. Jiang, L. Xie, X. Liu, T. Yin, Z. Tian, C. Wang and Y. Chen, Efficient hydrodeoxygenation of lignin-derived phenolic compounds by using Ru-based biochar catalyst coupled with silicotungstic acid, *Renewable Energy*, 2023, **202**, 1160–1168.

65 Z. Zhong, J. Li, M. Jian, R. Shu, Z. Tian, C. Wang, Y. Chen, N. Shi and Y. Wu, Hydrodeoxygenation of lignin-derived phenolic compounds over Ru/TiO2 catalyst: Effect of TiO_2 morphology, *Fuel*, 2023, **333**, 126241.